ELSEVIER

Journal of Power Sources 93 (2001) 1–7

JOURNAL OF POWER SOURCES

www.elsevier.com/locate/jpowsour

Synthesis and characterization of $Gd_{1-x}Sr_xMnO_3$ cathode for solid oxide fuel cells

Hee Sung Yoon*, Seung Woo Choi, Dokyol Lee, Byong Ho Kim

Division of Materials Science and Engineering, Korea University, 1, 5-Ka, Anam-Dong, Sungbuk-Ku, Seoul 136-701, South Korea

Received 24 March 2000; received in revised form 19 May 2000; accepted 22 May 2000

Abstract

$Gd_{1-x}Sr_xMnO_3$ ($0 \leq x \leq 0.6$) is synthesized as the cathode material for solid oxide fuel cells (SOFC) using a citrate process. Properties of the oxides such as the crystal structure, electrical conductivity, thermal expansion coefficient (TEC) and reactivity with 8 mol% yttria-stabilized zirconia (8YSZ) or $Ce_{0.8}Gd_{0.2}O_{1.9}$ (CGO) electrolyte are investigated. The crystal structure is orthorhombic ($0 \leq x \leq 0.3$), cubic ($0.4 \leq x \leq 0.5$) or tetragonal ($x=0.6$), as dictated by the composition. The electrical conductivity increases, but the activation energy for conduction decreases, with increasing Sr content. The TEC displays normal behavior for $x \geq 0.3$ and increases with increasing Sr content. When heated at 1300°C for 48 h, $Gd_{1-x}Sr_xMnO_3$ reacts with 8YSZ to produce $SrZrO_3$, but does not react at all with CGO. The cathodic polarization of the mixed cathode, $Gd_{0.6}Sr_{0.4}MnO_{3-\delta}$–CGO, is reduced with increase in the CGO content. The maximum power density is about 210 mW/cm^2 in the vicinity of 50 vol.% CGO in the mixed cathode at an operating temperature of 800°C.

Keywords: $Gd_{1-x}Sr_xMnO_3$; Citrate process; Solid oxide fuel cell; Electrical conductivity; Thermal expansion coefficient; Reactivity; Cathodic polarization; Three-phase boundary

1. Introduction

The solid oxide fuel cell (SOFC) is now considered to be a potential future energy system and is expected to substitute existing energy conversion systems which use fossil fuels. The SOFC, however, must be operated at high temperatures (around 1000°C) to achieve satisfactory power density. Such high-temperature operation causes various problems which include: sintering of electrodes, formation of an insulating layer at the electrode/electrolyte interface by interdiffusion, crack formation due to stresses caused by a large difference in the thermal expansion coefficients (TECs) of the cell components. It is, therefore, desirable to lower the operation temperature. This would not only solve the above-mentioned problems, but also extend the range of material selection for cell components such as the interconnector and the cell housing. The reduction of operation temperature can be achieved either by thinning the electrolyte layer [1,2] or by using highly conductive electrolytes such as ceria-based oxides [3].

$La_{1-x}Sr_xMnO_3$, one of the representative cathode materials for SOFCs, has been reported to form second phases like $La_2Zr_2O_7$ or $SrZrO_3$ at the interface where it contacts the YSZ electrolyte. The formation of second phases causes degradation in cell performance, since such phases usually have electrical conductivities which are two to three orders lower than that of YSZ. $La_{1-x}Sr_xCoO_3$, though it has higher conductivity than $La_{1-x}Sr_xMnO_3$, is known to have problems of high TEC ($>20\times10^{-6}$/°C) and phase instability at high temperatures. $La_{1-x}Sr_xFeO_3$ is similar to the YSZ electrolyte in its linear thermal expansion coefficient, but has a rather low electrical conductivity [4,5]. $La_{1-x}Sr_xCo_{1-y}Fe_yO_3$, which has been widely studied as a cathode material for low-temperature SOFCs, also suffers from chemical reaction with YSZ. $La_{1-x}Sr_xMn_{1-y}Co_yO_3$, known to have a high reducing power, is believed to form a second phase when the cobalt content is high [6].

In this study, $Gd_{1-x}Sr_xMnO_3$ [7] has been synthesized as the cathode material for SOFCs using a citrate process. Thereafter, its crystal structure, electrical conductivity, TEC, and reactivity with 8YSZ or CGO electrolytes have been investigated. Also, the cathodic polarization, which depends upon the content of CGO in the mixed cathode $Gd_{0.6}Sr_{0.4}MnO_{3-\delta}$–CGO, has been evaluated.

* Corresponding author. Tel.: +82-2-921-9237; fax: +82-2-921-9237.
E-mail address: heesung-yoon@hanmail.net (H.S. Yoon).

0378-7753/01/$ – see front matter
PII: S0378-7753(00)00504-8

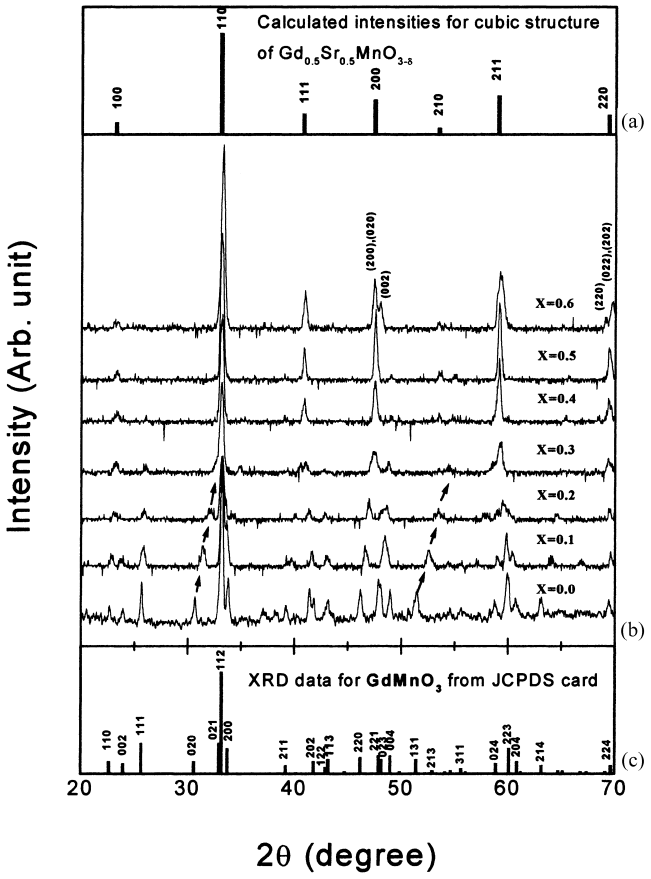

Fig. 1. X-ray diffraction patterns for $Gd_{1-x}Sr_xMnO_{3-\delta}$ ($0 \leq x \leq 0.6$) after firing at 1300°C for 5 h: (a) calculated intensities for cubic structure of $Gd_{0.5}Sr_{0.5}MnO_{3-\delta}$ from data (b) in this figure, and (c) intensities for $GdMnO_3$ from JCPDS card.

2. Experimental procedure

$Gd_{1-x}Sr_xMnO_3$ ($0 \leq x \leq 0.6$) powders were produced as the cathode material for SOFCs. For this purpose, polymeric precursors were synthesized using the citrate process [8,9] and calcined at 700°C for 2 h. $Gd(NO_3)_3 \cdot 6H_2O$ (99.95%), $Sr(NO_3)_2$ (99.9%) and $Mn(NO_3)_2 \cdot xH_2O$ (99.99%) from Aldrich were used as the starting materials. The calcined powder was reheated at 1300°C for 5 h in air for X-ray diffraction experiments. For other characterization, the powder was compacted into 8 mm diameter rods and sintered at 1400°C for 4 h.

Table 1
Crystal structure and lattice parameters of the $Gd_{1-x}Sr_xMnO_{3-\delta}$

Composition	Crystal structure	Lattice parameter (Å)		
		a	*b*	*c*
$GdMnO_3$	Orthorhombic	5.31	5.84	7.43
$Gd_{0.9}Sr_{0.1}MnO_{3-\delta}$	Orthorhombic	5.34	5.72	7.52
$Gd_{0.8}Sr_{0.2}MnO_{3-\delta}$	Orthorhombic	5.40	5.63	7.54
$Gd_{0.7}Sr_{0.3}MnO_{3-\delta}$	Orthorhombic	5.42	5.56	7.62
$Gd_{0.6}Sr_{0.4}MnO_{3-\delta}$	Cubic	3.84	3.84	3.84
$Gd_{0.5}Sr_{0.5}MnO_{3-\delta}$	Cubic	3.83	3.83	3.83
$Gd_{0.4}Sr_{0.6}MnO_{3-\delta}$	Tetragonal	3.83	3.83	3.81

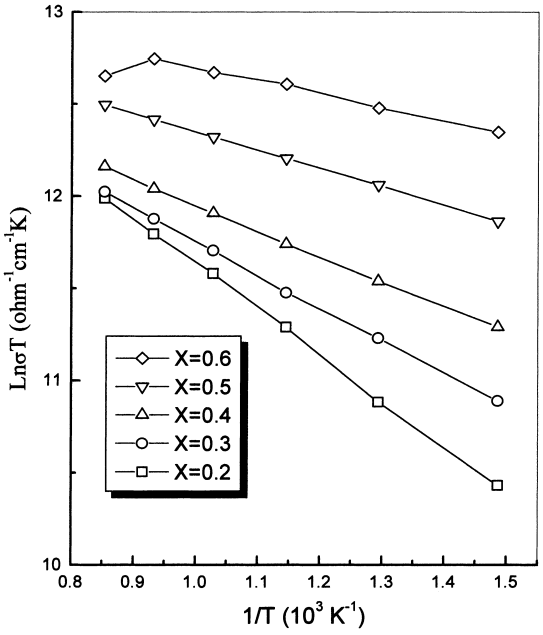

Fig. 2. Arrhenius plots of electrical conductivity of $Gd_{1-x}Sr_xMnO_{3-\delta}$ ($0.2 \leq x \leq 0.6$).

The crystal structures of the synthesized powders were determined from their XRD patterns measured on a Rigaku diffractometer (Geigerflex DMAX-II) using Cu Kα radiation. The electrical conductivity was measured at temperatures in the range of 400–900°C using the four-probe dc method. In the measurements dc currents of 1–100 mA were used. The linear thermal expansion was determined by thermomechanical analysis (TMA) using a Rigaku 811H instrument. Samples were heated at a rate of 5°C/min up to 900°C and quartz was used as the reference.

In order to study the reactivity of $Gd_{1-x}Sr_xMnO_3$ cathodes with electrolytes, the cathode and electrolyte powders were mixed in a 1:1 weight ratio, compacted, and heated at 1300°C for 48 h in air. The compact was then pulverized in a mortar and analyzed using XRD. Two electrolyte materials, 8YSZ and $Ce_{0.8}Gd_{0.2}O_{1.9}$, were used in this study. $Ce_{0.8}Gd_{0.2}O_{1.9}$ was synthesized from $Ce(NO_3)_3 \cdot 6H_2O$ and $Gd(NO_3)_3 \cdot 6H_2O$, using the same process as for $Gd_{1-x}Sr_xMnO_3$, but the calcination was carried out at 900°C for 1 h.

Table 2
Electrical conductivity at 800°C and activation energy of the $Gd_{1-x}Sr_xMnO_{3-\delta}$

Composition	Conductivity at 800°C (S/cm)	Activation energy (kJ/mol)
$Gd_{0.8}Sr_{0.2}MnO_{3-\delta}$	123.6	20.6
$Gd_{0.7}Sr_{0.3}MnO_{3-\delta}$	134.0	14.9
$Gd_{0.6}Sr_{0.4}MnO_{3-\delta}$	157.8	11.4
$Gd_{0.5}Sr_{0.5}MnO_{3-\delta}$	229.5	8.3
$Gd_{0.4}Sr_{0.6}MnO_{3-\delta}$	319.6	<5

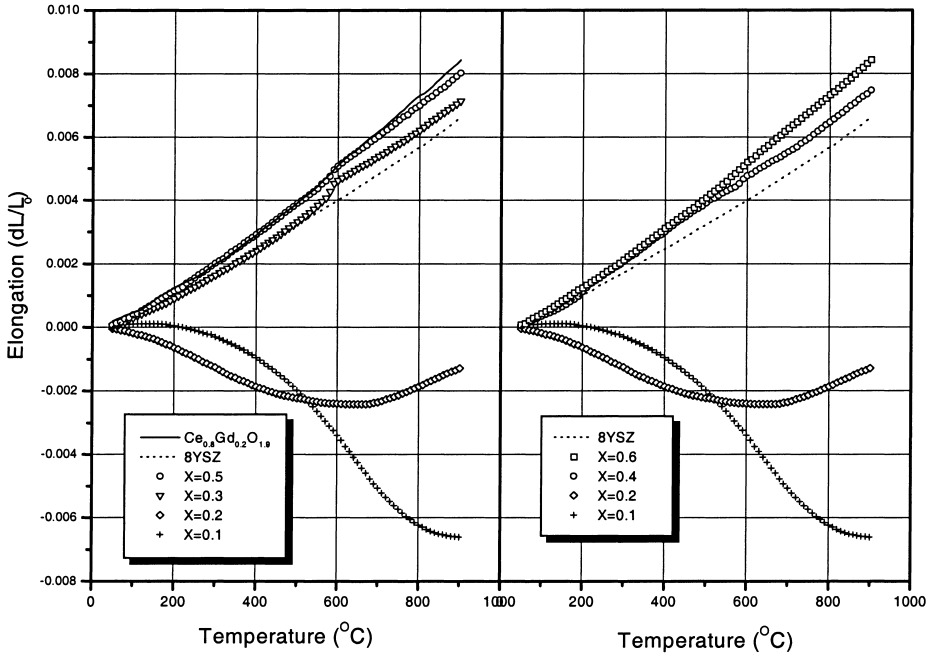

Fig. 3. TMA curves for $Gd_{1-x}Sr_xMnO_{3-\delta}$ ($0.1 \leq x \leq 0.6$), $Ce_{0.8}Gd_{0.2}O_{1.9}$ and 8YSZ sintered at 1400°C for 4 h (heating rate 5°C/min).

YSZ powder from Tosoh Corporation and NiO powder from Kanto were mixed in an approximate 40:60 weight ratio. The anode powders were then compacted under uniaxial pressure. Green anode substrates were subsequently baked at 900°C for 10 h. A YSZ electrolyte film was formed on a NiO–YSZ anode substrate by a colloidal coating method. The YSZ electrolyte/NiO–YSZ anode was then fired at 1400°C for 4 h. $Gd_{1-x}Sr_xMnO_3$ was mixed with CGO in proportions which ranged from 100:0 to 40:60. The $Gd_{1-x}Sr_xMnO_3$–CGO powder was then mixed with α-terpineol and dibutyle phtalate to form a paste, and the paste was coated on a YSZ/NiO–YSZ substrate and fired at

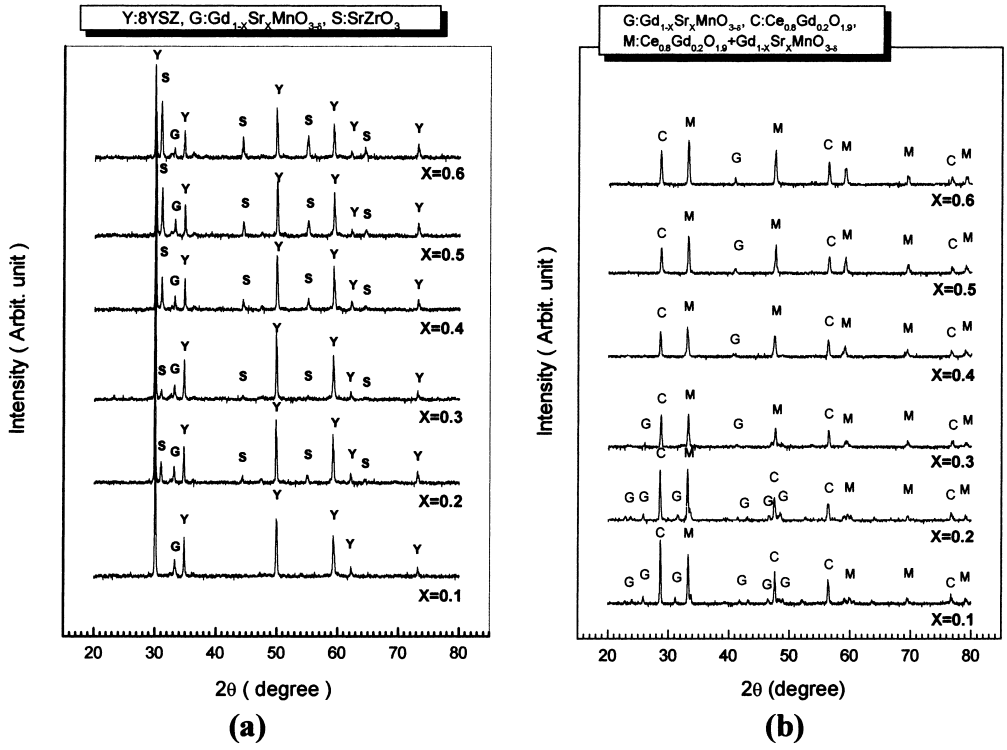

Fig. 4. XRD patterns for mixtures of (a) $Gd_{1-x}Sr_xMnO_{3-\delta}$($0.1 \leq x \leq 0.6$)/8YSZ and (b) $Gd_{1-x}Sr_xMnO_{3-\delta}$($0.1 \leq x \leq 0.6$)/$Ce_{0.8}Gd_{0.2}O_{1.9}$ after firing at 1300°C for 48 h.

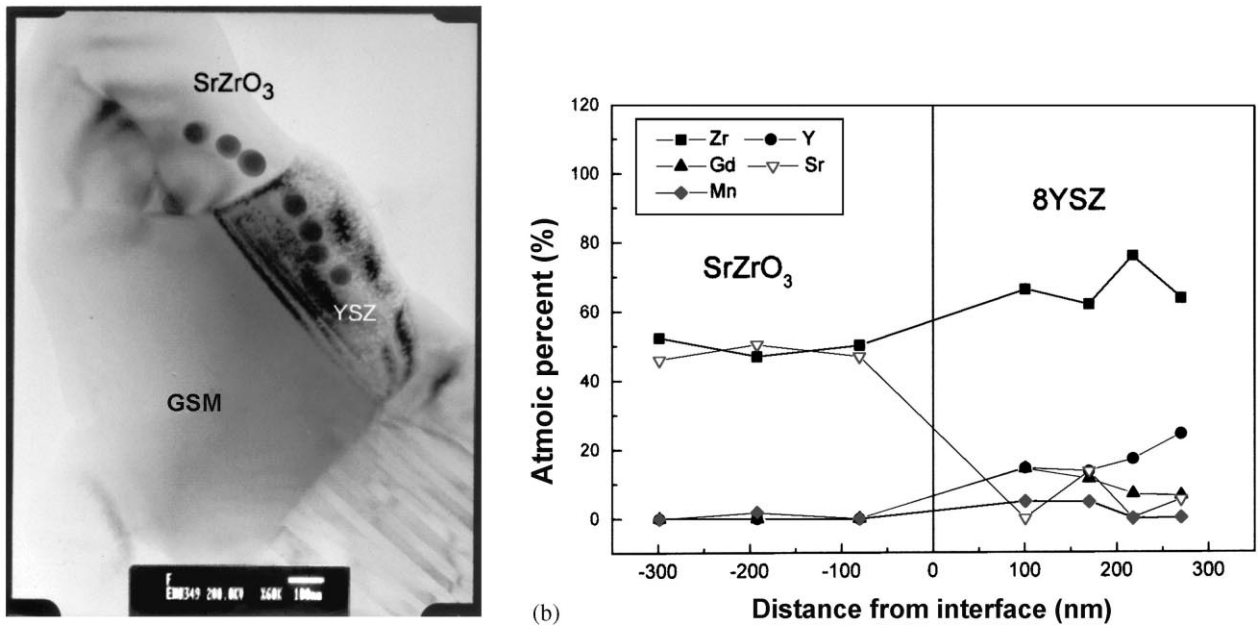

Fig. 5. HRTEM/EDX analysis of 8YSZ/$Gd_{0.5}Sr_{0.5}MnO_{3-\delta}$ mixture after sintering at 1300°C for 48 h: (a) HRTEM image and (b) concentration profile for vicinity of interface.

1400°C for 4 h. Platinium mesh was used as the current-collector, which was fixed to the electrode surface by means of silver paste from Dupont.

3. Results and discussion

The X-ray diffraction patterns for $Gd_{1-x}Sr_xMnO_3$ with various Sr contents are presented in Fig. 1, together with those calculated for a cubic $Gd_{0.5}Sr_{0.5}MnO_3$ phase and constructed from JCPDS data for an orthorhombic $GdMnO_3$ phase. The crystal structure of $Gd_{1-x}Sr_xMnO_3$ is orthorhombic for $0 \leq x \leq 0.3$. As the amount of Sr increases, however, the peak intensities decrease and (0 2 0) and (1 3 1) peaks are shifted to the high angle side. This shift is thought to be due to a decrease in the lattice parameter *b*. After all these preparatory stages, the $Gd_{1-x}Sr_xMnO_3$ phase becomes cubic when $x=0.4$ or 0.5. Finally, it turns into a tetragonal

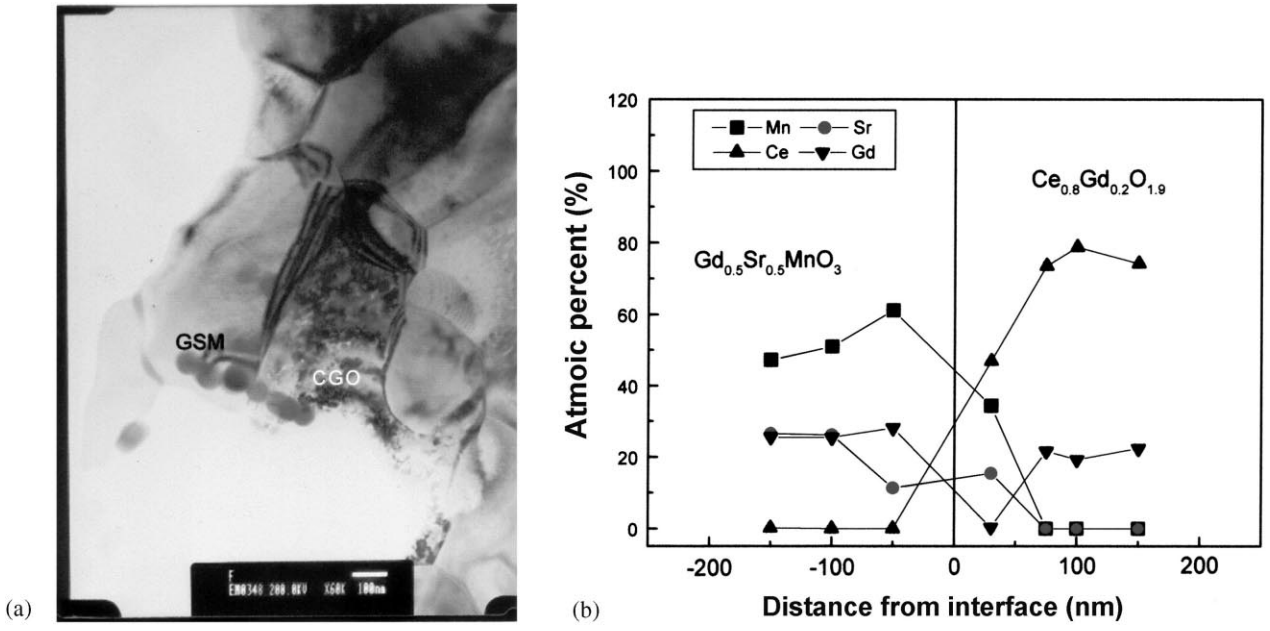

Fig. 6. HRTEM/EDX analysis of $Ce_{0.8}Gd_{0.2}O_{1.9}$/$Gd_{0.5}Sr_{0.5}MnO_{3-\delta}$ mixture after sintered at 1300°C for 48 h: (a) HRTEM image, and (b) concentration profile for vicinity of interface.

structure when x=0.6, which can be recognized by the split of (2 0 0) and (2 2 0) cubic peaks. The crystal structures and their lattice parameters for $Gd_{1-x}Sr_xMnO_3$ phases are summarized in Table 1.

Arrehnius plots for the electrical conductivity of $Gd_{1-x}Sr_xMnO_3$ ($0.2 \leq x \leq 0.6$) are given in Fig. 2. The conductivities, σ, were measured in the temperature range 400–900°C in air. The activation energies for conduction were determined from the plots, using the following expression derived for the small polaron mechanism [10,11]:

$$\sigma = \frac{A}{T} \exp\left(\frac{-E_a}{\kappa T}\right) \quad (1)$$

where A is the preexponential factor, κ the Boltzmann constant, T the absolute temperature and E_a the activation energy. It can be seen from the data in Fig. 2 and Table 2 that the electrical conductivity increases, but the activation energy decreases, with increasing Sr content. Also, most of $Gd_{1-x}Sr_xMnO_3$ materials show the conducting behaviour of semiconductors, except the one with x=0.6 which displays metallic conduction at high temperatures. The highest conductivity was about σ=320 S/cm at 800°C, which is similiar to or higher than that of $La_{1-x}Sr_xMnO_3$.

The temperature dependence of thermal expansion of $Gd_{1-x}Sr_xMnO_3$ is presented in Fig. 3. The thermal expansion of 8YSZ and CGO is also shown for comparison. The thermal expansion coefficients of $Gd_{0.9}Sr_{0.1}MnO_3$ and $Gd_{0.8}Sr_{0.2}MnO_3$ are negative. For $Gd_{1-x}Sr_xMnO_3$ with $x \geq 0.3$, however, the thermal expansion exhibits a normal behavior similar to that of $La_{1-x}Sr_xMnO_3$, 8YSZ and CGO and the coefficient increases with increasing Sr content.

The XRD patterns for $Gd_{1-x}Sr_xMnO_3$/8YSZ and $Gd_{1-x}Sr_xMnO_3$/CGO mixtures reacted at 1300°C for 48 h in air are given in Fig. 4. While a second phase of $SrZrO_3$ is formed in the former, none is formed in the latter.

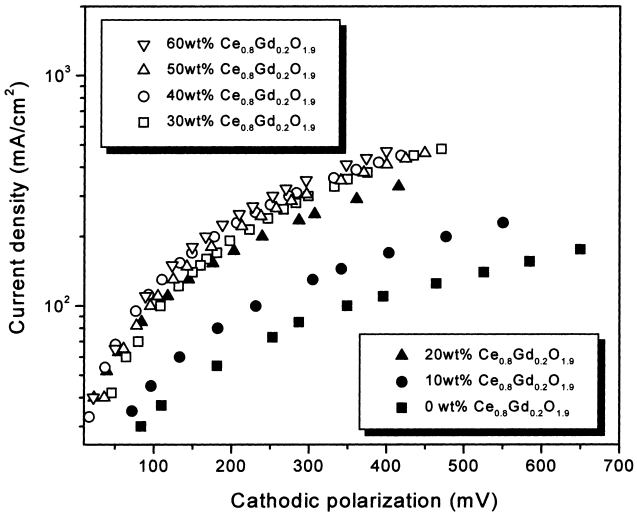

Fig. 8. Cathodic polarization of air, $Gd_{0.6}Sr_{0.4}MnO_{3-\delta}$–$Ce_{0.8}Gd_{0.2}O_{1.9}$/8YSZ/Ni–8YSZ, ($H_2$/$H_2O$) unit cell tested at 800°C according to the content (wt.%) of $Ce_{0.8}Gd_{0.2}O_{1.9}$ in $Gd_{0.6}Sr_{0.4}MnO_{3-\delta}$–$Ce_{0.8}Gd_{0.2}O_{1.9}$.

The results of HRTEM/EDX analyses for $Gd_{1-x}Sr_xMnO_3$/8YSZ and $Gd_{1-x}Sr_xMnO_3$/CGO mixtures are shown in Figs. 5 and 6, respectively. The above statement on the second phase formation at the interface was again confirmed.

A unit cell with a configuration of (H_2/H_2O), Ni–YSZ/YSZ/$Gd_{0.6}Sr_{0.4}MnO_{3-\delta}$–CGO mixed cathode, air was evaluated in terms of its current–voltage (*I–V*) characteritics. The open-circuit voltage (OCV) obtained for single cell tested at 800°C was about 1.0 V. The *I–V* curves, cathodic polarization and power densities according to a difference in the content of CGO in the cathode at an operating temperature of 800°C are shown in Figs. 7–9, respectively. The cathodic polarization is reduced and the maximum power

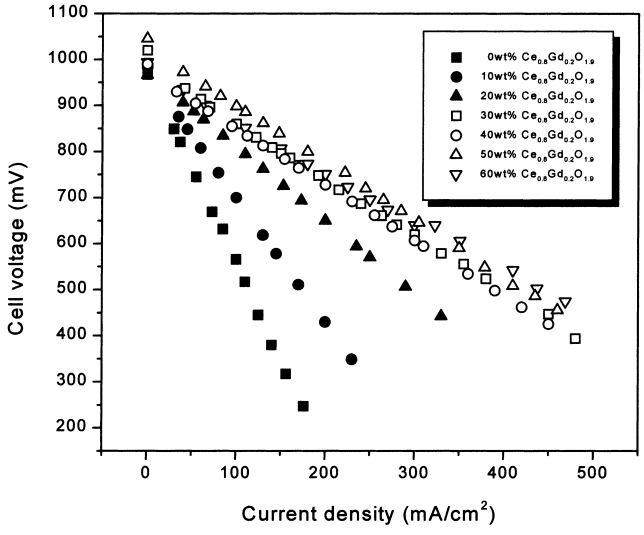

Fig. 7. Cell voltage of air, $Gd_{0.6}Sr_{0.4}MnO_{3-\delta}$–$Ce_{0.8}Gd_{0.2}O_{1.9}$/8YSZ/Ni–8YSZ, ($H_2$/$H_2O$) unit cell tested at 800°C according to the content (wt.%) of $Ce_{0.8}Gd_{0.2}O_{1.9}$ in $Gd_{0.6}Sr_{0.4}MnO_{3-\delta}$–$Ce_{0.8}Gd_{0.2}O_{1.9}$.

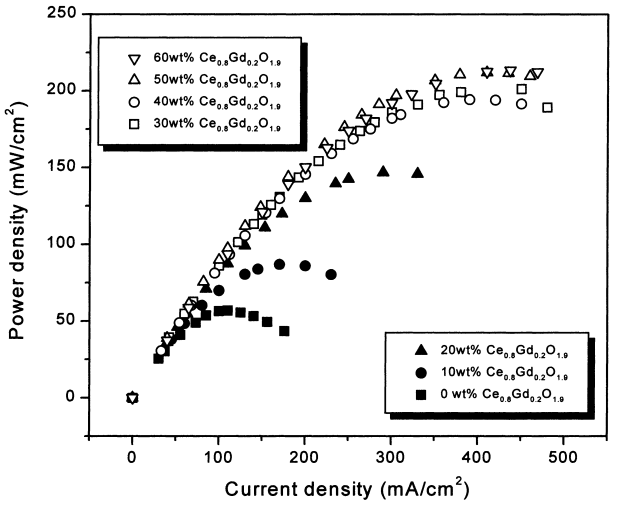

Fig. 9. Power density of air, $Gd_{0.6}Sr_{0.4}MnO_{3-\delta}$–$Ce_{0.8}Gd_{0.2}O_{1.9}$/8YSZ/Ni–8YSZ ($H_2$/$H_2O$) unit cell tested at 800°C according to the content (wt.%) of $Ce_{0.8}Gd_{0.2}O_{1.9}$ in $Gd_{0.6}Sr_{0.4}MnO_{3-\delta}$–$Ce_{0.8}Gd_{0.2}O_{1.9}$.

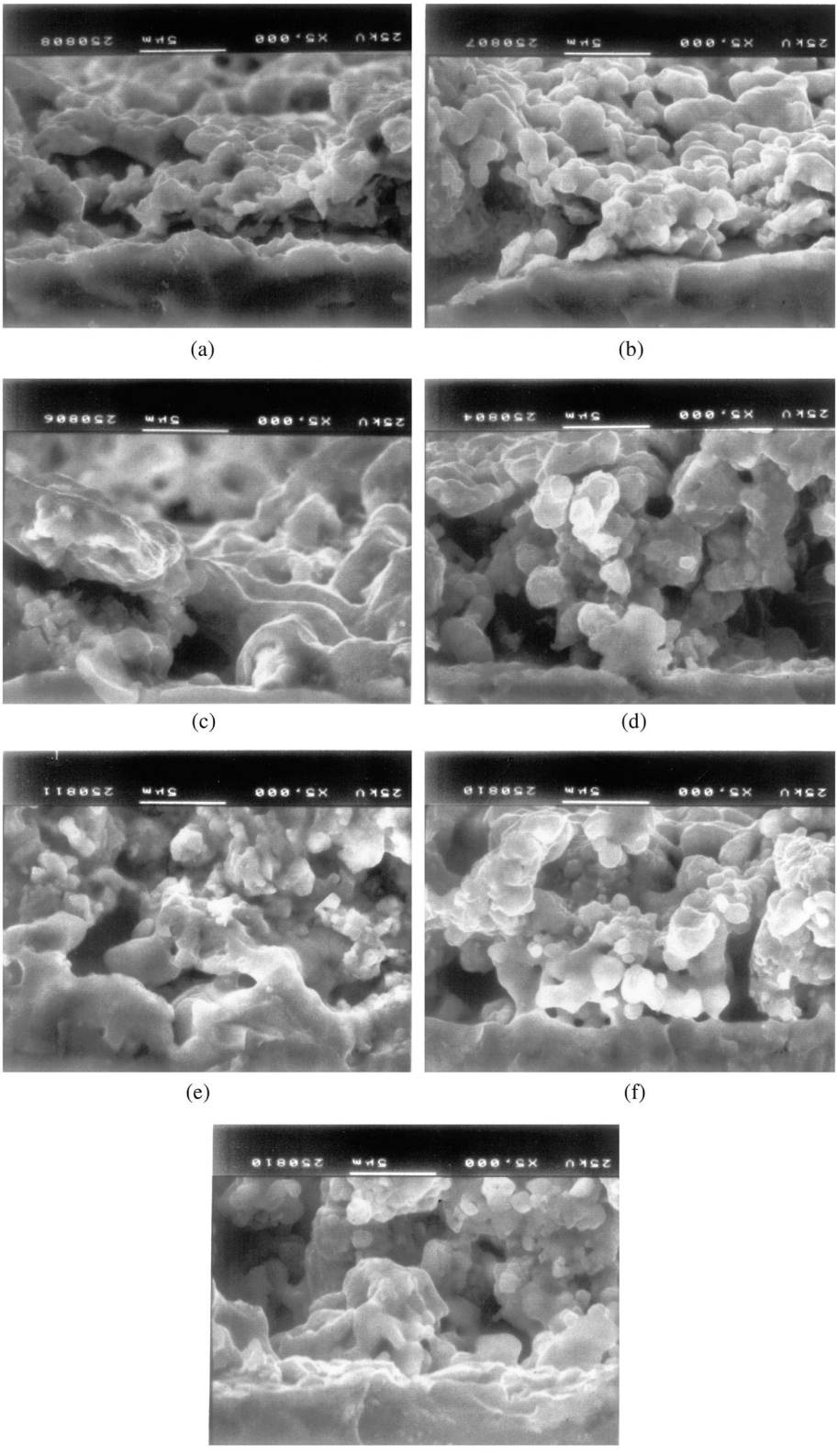

Fig. 10. SEM micrographs of cross-section fracture of $Gd_{0.6}Sr_{0.4}MnO_{3-\delta}$–$Ce_{0.8}Gd_{0.2}O_{1.9}$ cathodes for $Ce_{0.8}Gd_{0.2}O_{1.9}$ powder at (a) 0%; (b) 10%; (c) 20%; (d) 30%; (e) 40%; (f) 50% and (g) 60% of the total weight after firing at 1400°C for 4 h.

density is increased with CGO content in the $Gd_{0.6}Sr_{0.4}MnO_{3-\delta}$–CGO mixed cathode. The maximum power density is about 210 mW/cm^2 (485 mV, 435 mA) for the cathode including 50–60 wt.% CGO. The mixing of CGO in cathode enlarged the three-phase boundary (electrolyte/cathode/air) length.

The microstructure of the $Gd_{0.6}Sr_{0.4}MnO_{3-\delta}$–CGO mixed cathode is shown in Fig. 10. As the content of CGO increases, the size of the cathode particles is reduced.

4. Conclusions

$Gd_{1-x}Sr_xMnO_3$ ($0 \leq x \leq 0.6$) has been synthesized as the cathode material for SOFCs using a citrate process. The crystal structure was orthorhombic ($0 \leq x \leq 0.3$), cubic ($0.4 \leq x \leq 0.5$), and tetragonal ($x=0.6$) as dictated by the composition. The electrical conductivity increases, but the activation energy for conduction decreases with increasing Sr content. The thermal expansion shows normal behaviour for $x \geq 0.3$ and the coefficient increases with increasing Sr content. When heated at 1300°C for 48 h, $Gd_{1-x}Sr_xMnO_3$ reacts with 8YSZ to produce a second phase of $SrZrO_3$, but does not react at all with CGO. The cathodic polarization of a $Gd_{0.6}Sr_{0.4}MnO_{3-\delta}$–CGO mixed cathode is reduced as the CGO content is increased. The maximum power density is about 210 mW/cm^2 in the vicinity of 50 vol.% CGO in a $Gd_{0.6}Sr_{0.4}MnO_{3-\delta}$–CGO mixed cathode.

Acknowledgements

Financial support from Korean Ministry of Education Research Fund for Advanced Material '96 (the second year) is gratefully acknowledged.

References

[1] T. Ishihara, T. Kudo, H. Matsuda, Y. Takita, in: S.C. Singhal, H. Iwahara (Eds.), Solid Oxide Fuel Cells/1993, PV 93-4, The Electrochemical Society Proceeding Series, Pennington, NJ, 1993, p. 65.
[2] S. Souza, S.J. Visco, C. Jonghe, Solid State Ionics 98 (1997) 57.
[3] D.Y. Wang, A.S. Nowick, J. Electrochem. Soc. 126 (7) (1979) 1155.
[4] L-W. Tai, M.M. Nasrallah, H.U. Anderson, in: S.C. Singhal, H. Iwahara (Eds.), Solid Oxide Fuel Cells/1993, PV 93-4, The Electrochemical Society Proceeding Series, Pennington, NJ, 1993, p. 241.
[5] C.C. Chen, M.M. Nasrallrah, H.U. Anderson, The Electrochemical Society Proceeding Series, Pennington, NJ, 1993, p. 252.
[6] G. Stochniol, A. Gupta, A. Naoumidis, D. Stover, in: U. Stimming, S.C. Singhal, H. Tagawa, W. Lehnert (Eds.), Solid Oxide Fuel Cells/1997, PV 97-40, The Electrochemical Society Proceeding Series, Pennington, NJ, 1997, p. 888.
[7] Y. Taketa, H.Y. Tu, H. Sakaki, S. Watanabe, N. Imanishi, O. Yamamoto, M.B. Phillipps, N.M. Sammes, J. Electrochem. Soc. 144 (8) (1997) 2810.
[8] M. Pechini, US Patent 3, 330, 697 (1967).
[9] I.Y. Yoon, H.S. Yoon, B.H. Kim, J. KIEEME 11 (1) (1998) 18.
[10] J.A.M. van Roosmalen, J.P.P. Huijsmans, L. Plom, Solid State Ionics 66 (1993) 279.
[11] P.A. Cox, The Electronic Structure and Chemistry of Solid, Oxford University Press, New York, 1987, p. 179.